Electronic Supplementary Information: Near-zero surface pressure assembly of rectangular lattices of microgels at fluid interfaces for colloidal lithography

Miguel Angel Fernandez-Rodriguez,[a,b*] Maria-Nefeli Antonopoulou,[b,c] and Lucio Isa[b]

Microgel synthesis

We synthesized PNIPAM microgels by precipitation polymerization [1]. We started from 180 mM of N-isopropylacrylamide (NIPAM, TCI 98.0%) monomer solutions in MilliQ water, after purification and recrystallization in a hexane/toluene mixture. We then added the crosslinker N-N'-Methylenebisacryl-amide (BIS, Fluka 99.0%) in different ratios, i.e. at 3, 5, and 7 wt%, respectively adjusting the volumes to have a constant total mass of monomers. The solution was kept at 80 °C under N_2 atmosphere and the initiator potassium persulfate (KPS, Sigma-Aldrich 99.0%) was added at 1.8 mM to initiate the reaction, keeping the temperature constant for 5 h. Next, the dispersion was cleaned three times by ultracentrifugation at 20000 rpm for 1 h. At the end of each ultracentrifugation cycle, the supernatant was replaced with MilliQ water, and the microgels were re-dispersed by 1 h of ultrasonication. These microgels present a core-shell architecture, with a more crosslinked core and a less crosslinked shell [1]. The size of the particles can be increased, while keeping the same crosslinking ratio, by growing an extra shell. The reaction proceeds similarly to the one described above where the microgels are dispersed along the extra NiPAm and BIS monomers. The monomers were added in four steps by adding 1 mL of 1.2 mM KPS in MilliQ water and 1.25 mL of the crosslinker-monomer solution every 10 minutes. Afterwards, the synthesis and cleaning proceed as described before. We label our particles as CXSY, where X = 3,5,7 is the crosslinking mass ratio and Y=0 or 1 indicates the presence of an extra shell [2]. Additionally, we used a microgel with methacrylic acid co-monomer, P(NIPAM-co-MAA), synthesized as described in a previous publication [3] for the realisation of the sequential depositions. The sizes of all microgels in bulk MilliQ-water were measured by dynamic light scattering (DLS, Malvern Zetasizer) at 25 °C. The diameter of isolated microgels deposited on silicon wafers (see next section for details on the deposition process) from the water/hexane interface were measured with atomic force microscopy (AFM, Brucker Icon Dimension) in tapping mode (300 kHz, $26 mN/m$) at a rate of 1 Hz (see Table S1).

Microgel	$2R_h\,(nm)$	$2R_{AFM}\,(nm)$
C7S1	620 ± 204	1202 ± 47
C7S0	574 ± 73	786 ± 30
C5S1	620 ± 204	1066 ± 71
C5S0	597 ± 127	882 ± 30
C3S1	879 ± 121	1578 ± 46
C3S0	618 ± 83	1095 ± 66
P(NIPAM-co-MAA)	213 ± 10	546 ± 50

Table S1: Hydrodynamic diameter $2R_h$ of the microgels in bulk (DLS), and at the interface (from 25 isolated deposited microgels, by AFM).

[a] *Laboratory of Surface and Interface Physics, Biocolloids and Fluid Physics group, Department of Applied Physics, Faculty of Sciences, University of Granada, Campus de Fuentenueva s/n, ES 18071 Granada, Spain. E-mail: mafernandez@ugr.es*

[b] *Laboratory for Soft Materials and Interfaces, Department of Materials, Swiss Federal Institut of Technology Zürich, Vladimir-Prelog-Weg 1-5/10, 8093 Zürich, Switzerland.*

[c] *Current address: Polymeric Materials, Department of Materials, Swiss Federal Institut of Technology Zürich, Vladimir-Prelog-Weg 1-5/10, 8093 Zürich, Switzerland.*

Compression curve and depositions on silicon substrates at fixed Π

Microgels were deposited on 2x2 cm^2 silicon substrates (Siltronix, $< 100 >$) as reported in previous works[2–5]. The silicon substrates (Siltronix, $< 100 >$ orientation, 100 mm single polished side, p-type, boron-doped, $3-6\,cm$) were cut into 2x2 cm^2 pieces with a diamond pen, cleaned in ultrasonic baths of toluene (Fluka Analytical, 99.7%), isopropanol (IPA, Fisher Chemical, 99.97%) and MilliQ water, and dried with N_2. The clean substrate was placed on the dipping arm of a liquid-liquid Langmuir-Blodgett trough (KSV5000, Biolin Scientific), at an orientation of 30° relative to the interface. We filled the trough with MilliQ water, keeping the substrate fully immersed, and cleaned the interface by closing the barriers and measuring the surface pressure Π with a Wihelmy plate. Whenever $\Pi > 0.4\,mN/m$, we vacuum cleaned the interface and opened the barriers, zeroed Π and repeated the process again. Next, 100 mL of n-hexane (Sigma-Aldrich, HPLC grade 95%, used as received) were added to create the water/hexane interface. Next, we raised the substrate until it barely crossed the water/hexane interface and zeroed the surface pressure Π. This position on the substrate is used a reference to estimate the value of Π vs position. Next, we mixed 0.1 wt% of the microgel suspensions in 4:1 suspension:IPA, where IPA acts as spreading agent at the interface. We then added the microgel dispersion at the interface with a Hamilton glass microsyringe (100 μL) and let the system stabilize for 10 minutes. Finally, for the compression curve Π was gradually increased by compressing the interface with the barriers while the substrate was raised to deposit the monolayer at the same time. In the case of depositions with fixed Π, the position of the barrier is adjusted while the substrate was raised through the interface by the feedback of the Langmuir-Blodgett trough. The area per particle A_p of the deposited monolayers for the compresion curve in Fig. 2 was obtained via optical microscopy (Zeiss Axio Imager Z1 Upright microscope) with a 63x objective and images taken with an AxioCam camera, processed with the open source software ImageJ. For the calculation of the Ψ_4 and Ψ_6 values a custom made python program using the freud package was used[6]. See Fig. S1 for an AFM characterisation of the square lattices. In this AFM image, it is worth noting that the standard deviation of a height profile on the periphery of a microgel is $\approx 0.6\,nm$. This value is compatible with the amplitude of the capillary deformation $H_{1,2} = 0.4\,nm$ estimated in the main text for a microgel at the water/oil interface, to explain a quadrupolar interaction of order K_BT. Thus, the roughness induced by the dangling polymers at the outermost part of the microgels at the interface might be enough to provide the quadrupolar capillary interaction that we observe.

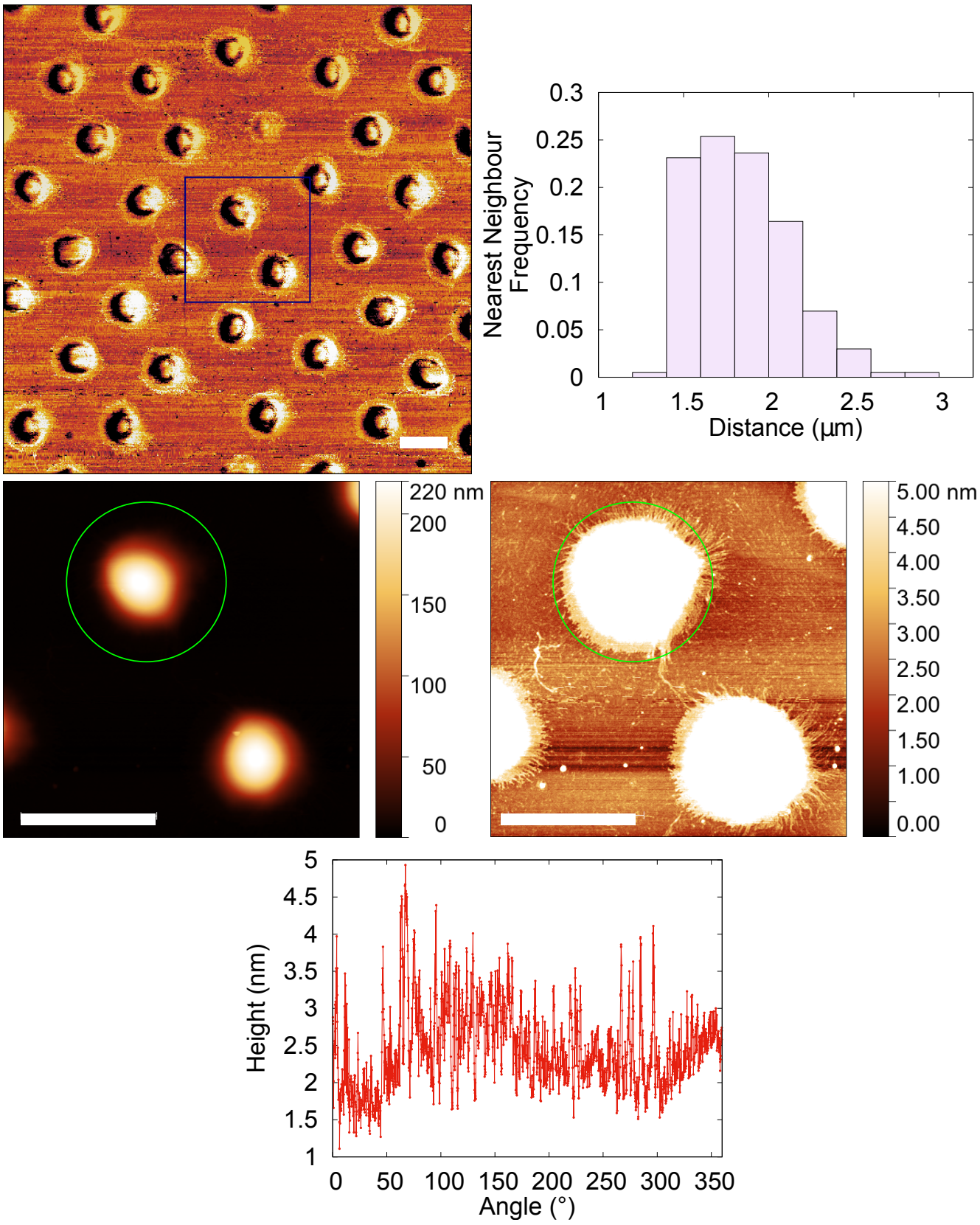

Figure S1: AFM phase image of square lattices obtained by depositing C7S1 microgels at $\Pi \approx 0 mN/m$. The histogram of nearest neighbours distribution shows distances clearly larger than the diameter reported in Table S1 and visible from the AFM images, with an average value of $(1.8 \pm 0.3)\,\mu m$. The AFM height images below are zoomed images, corresponding to the square marked in the image above. The height image on the left spans over the full height range while the one on the right is constrained to 5 nm-height to visualize the dangling polymers. A height profile is extracted at the green circle, which it is represented in the image below, with an average and standard deviation of $(2.5 \pm 0.6)\,nm$, and a maximum height difference of $3.8\,nm$. All scale bars are $1\,\mu m$.

Imaging the microgels in situ at interfaces

Real-time imaging

For the real time imaging we used two setups. One involves a custom-built liquid-liquid Langmuir trough (based on a KSV Nima medium trough) where the microgels are imaged with an upright microscope (Nikon LV-FM microscope equipped with a 40x dipping objective and a Coolsnap Dyno Mono camera - Movie S1, acquired at 10 fps). The ring that we used to restrict convection at the interface was 3D-printed with a Nanoscribe Professional GT device. The ring was designed in openscad (see Fig. S2a), printed and developed, cured under UV light for 2 days, glued to a tungsten filament of $58\,\mu m$-diameter with araldite, micromanipulated with two micro-robots (miBOT, Imina Technologies, see Fig. S2b) and placed on a C7S1 microgel-laden water/hexadecane interface (see Fig. S2c-d). The second setup uses a conventional cell made of a big coverslip as a base, a smaller coverslip with a circular opening made by a laser cutter, and a metal ring on top. The three parts are glued together with UV glue. This enables to fill the well made between the two bottom coverslips with water, then the microgels are deposited and finally the cell is filled with hexadecane (Sigma Aldrich 99%) and closed with another coverslip. Using a thin water well and a thin bottom glass enables to image the microgels at the interface with with an inverted microscope (Zeiss Axio Observer Z1) using a 63x objective and acquiring images with a camera (sCMOS Andor Zyla) at 10 fps and 10 ms exposure time an inverted microscope using a 63x objective (Movie S2 and S3, recorded at 10 fps. Drift is substracted from the movies). No significant differences are expected between hexane and hexadecane due to similar interfacial tension and PNIPAM solubility.

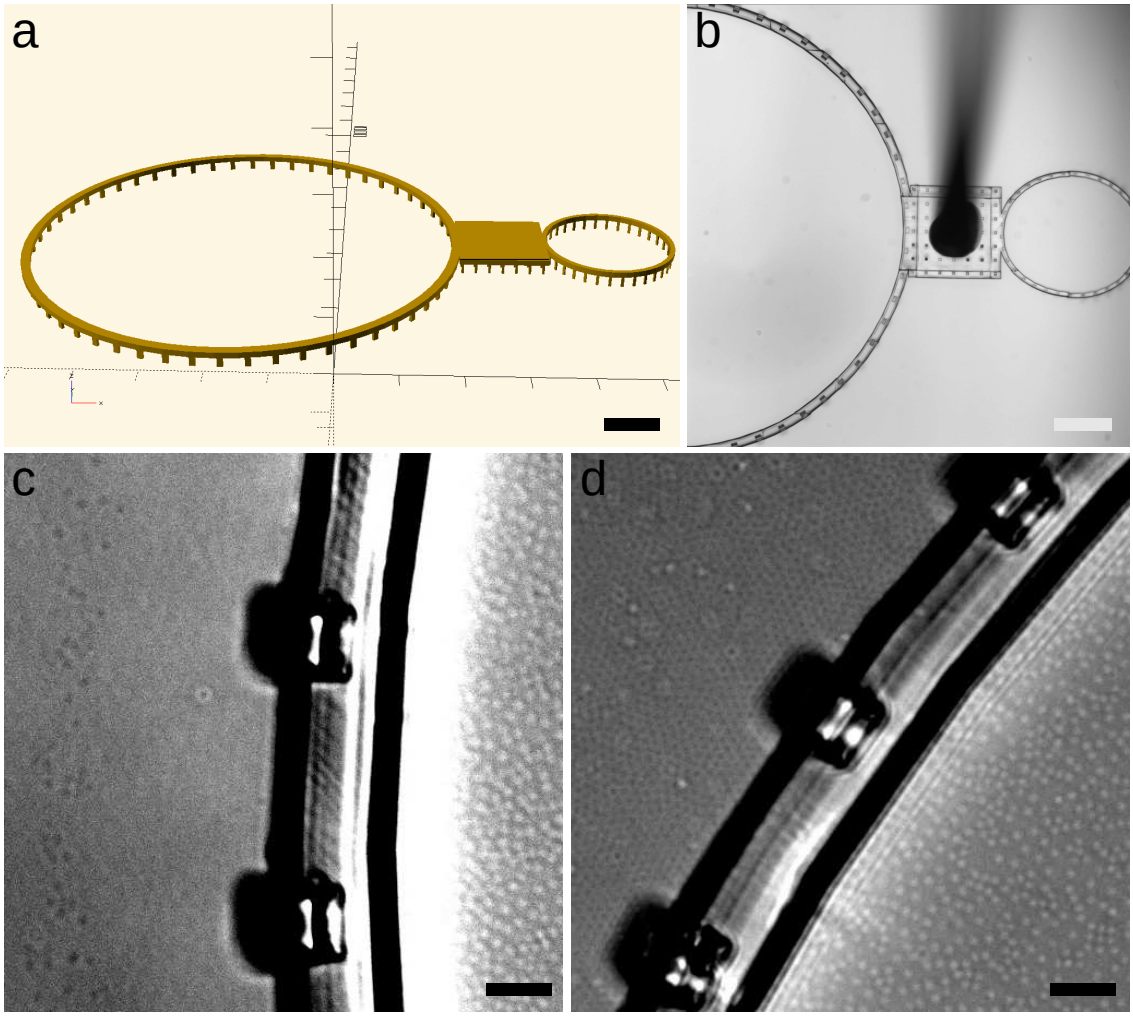

Figure S2: **(a)** Openscad model of the ring printed using the Nanoscribe GT2. The pillars are necessary to remove the device from the substrate where it is printed. The larger ring is used in the experiment. **(b)** Ring as printed, developed, cured over 2 days and connected to a $58\,\mu m$-diameter tungsten filament glued with araldite (the glue is visible as the black spot on the device). **(c-d)** Two different pictures during the same experiment with a C7S1 microgel-laden water/hexadecane interface imaged with a 40x dipping objective. In both pictures the right part is inside the ring. The left part shows a wide variation of A_p, ranging from sparse microgels (c) to a full monolayer (d) due to the convection flows present in the system. Scale bars are $100\,\mu m$ for (a-b) and $10\,\mu m$ for (c-d).

Freeze-fracture shadow-casting cryo-SEM

The freeze-fracture shadow-casting (FreSCa) cryo-SEM technique was used to image microgels at a water/decane (Sigma-Aldrich, 99%) interface as described in a previous work[1]. No significant differences are expected with hexane, as with hexadecane, due to similar interfacial tension and PNIPAM solubility. Microgel-laden interfaces were prepared by pipetting $0.5\,\mu L$ of the desired microgel dispersion at 0.1 wt% into a $1\,mm^2$ copper holder and then covering it with $3\,\mu L$ of decane purified in a basic alumina column. A second flat copper top enclosed the interface and the copper "sandwich" was vitrified with a propane jet freezer (Bal-Tec/Leica JFD 030) and fractured under high-vacuum and cryogenic conditions (Bal-Tec/Leica VCT010 and Bal-Tec/Leica BAF060). The system breaks at the weakest point, which is the water/decane interface, exposing the microgels protruding from the water phase. Next, we deposited 2 nm of tungsten forming a 30°-angle with the interface and imaged the sample in a cryo-SEM (Zeiss Leo 1530). As none of the microgels cast any shadow, this ensures the contact angle is $< 30°$. This confirms that they are hydrophilic and that the portion protruding into decane collapses due to poor solubility. In Fig. S3, we show square lattices found for different microgels.

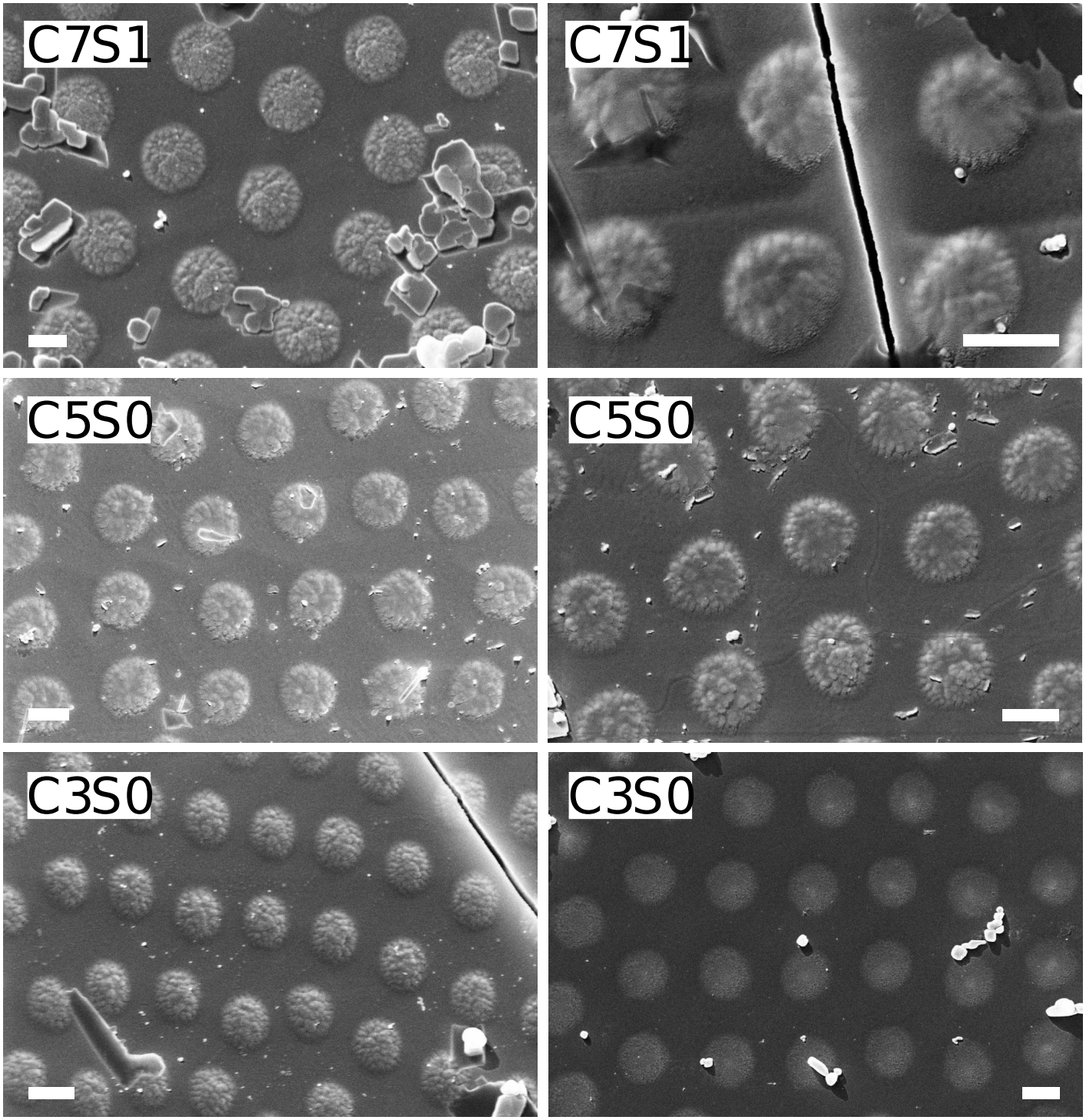

Figure S3: Cryo-SEM images of microgels at interfaces small domains with square lattices. Scale bars are $500nm$.

Curing the interface to characterize it via AFM and SEM

A C7S1 microgel-laden water/air interface created at $\Pi \sim 0$ in a teflon beaker (see Fig. S4a) was cured by exposing it to cyanoacrylate vapour overnight[7]. We deposit the cured interface onto a $2x2\,cm^2$ silicon substrate that was immersed in the water phase previous to the deposition of the microgels at the interface. The substrate is tilted 30° with the interface with a teflon holder and it could be moved using the yellow magnets in the picture. After exposure to the cyanoacrylate vapour, the substrate was raised and the cured interface deposited

on the silicon wafer. After transfer, the film ruptured in several locations, enabling the observation of the particles from the side (see Fig. S4b) and from below (see Fig. S4c-d, showing the portion of the microgels that was originally immersed in water). We observed square lattices in these cured surfaces with core-core distances compatibles with the histogram in Fig. S1.

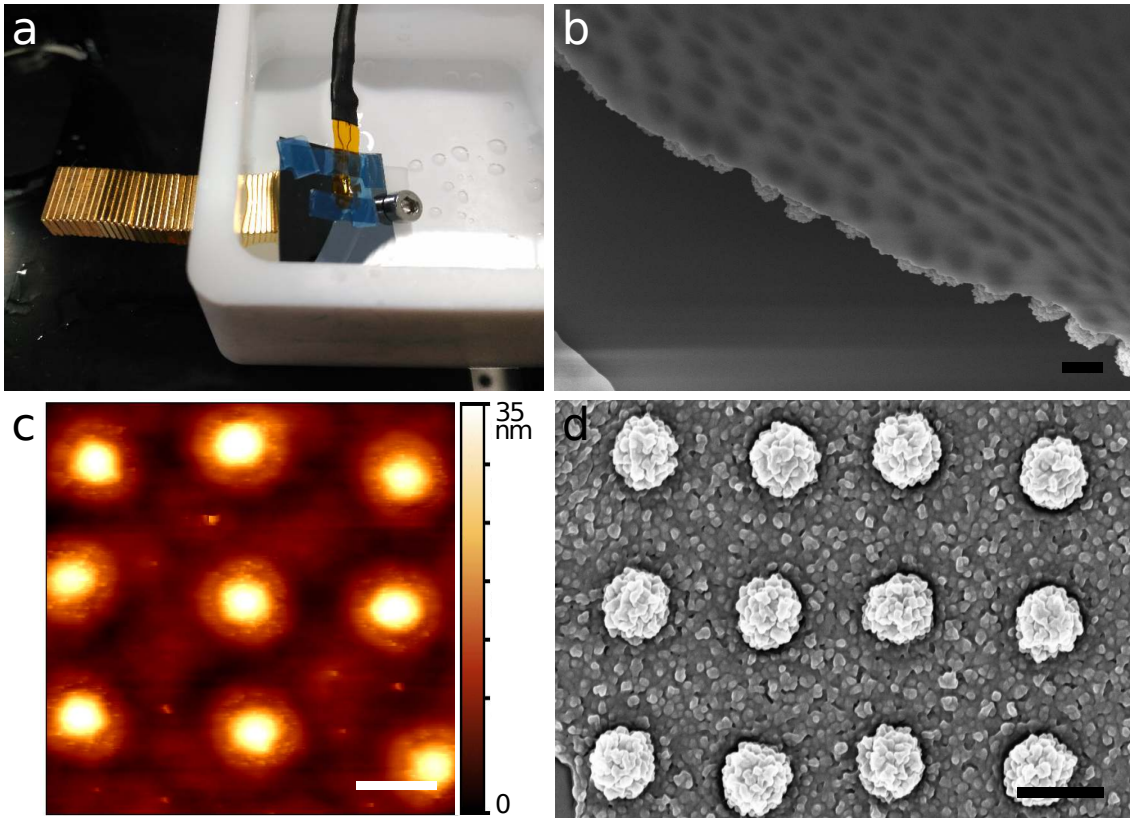

Figure S4: C7S1 microgel-laden water/air interface cured with cyanoacrylate. **(a)** Teflon beaker with an immersed $2x2\,cm^2$ silicon substrate, tilted by 30° relative to the interface and movable using the yellow magnets. The water temperature was measured with a thermocouple. **(b)** SEM image of a ruptured piece of the cured surface affording a lateral view of the film and the part of the microgels protruding into the water phase below the interface. **(c)** AFM height image of a cured microgel-laden water/air interface after exposure to cyanoacrylate **(d)** SEM image of an upside-down fragment of the microgel-cyanoacrylate film, showing the portion of the microgels that were immersed in water, with the microgels in a square lattice configuration. Scale bars $1\,\mu m$.

Soft colloidal lithography

Once the microgel monolayer is deposited on a silicon wafer, the microgels are very flat, as can be seen by Fig. 4a, where the maximum height of the microgels is 150 nm. This is often not enough to act to provide a sufficient masking for etching processes. We increased their thickness by exposing them to photoresist (AZ1518, MicroChemicals GmbH)[8] for 30 min, baking the substrate at $100^{\circ}C$ for 1 min and rinsing the excess of photoresist with acetone. This mechanism relies on the ability of the microgels to be swollen by the photoresist dissolved in ethanol, and after baking, on the different rate of removal of the photoresist by acetone, being slower for the photoresist inside the microgel. The final result is that the microgels increase their thickness. For example, for C7S0 the height increases from the $150\,nm$ reported in Fig. 4a to $\sim 500\,nm$, which it is comparable to the height provided by conventional spin coating of AZ1505 photoresist. Therefore, this intermediate step of swelling enables their use as etching masks in both metal-assisted chemical wet etching (MACE), and in deep reactive ion exchange dry etching (DRIE). For MACE, after swelling in photoresist, a $10\,nm$ layer of gold is sputter coated (Safematic CCU-010). Next, the substrate is submerged in the wet etching solution containing 3:3:2:2 solution of MilliQ water:ethanol:HF:H_2O_2 (ethanol from Fluka Analytical, 99.8%; HF from Sigma Aldrich, 48%; H_2O_2 from Merck 30%). Next, the substrate is rinsed in 1:4:40 of I_2:KI:MilliQ water (I_2 and KI from Sigma Aldrich, 99 %) to remove the gold layer, and subsequent rinsing in ethanol and acetone (Sigma Aldrich, 99 %). Next, for big aspect ratio-pillars, a CO_2 supercritical drier (Autosamdri-931, Tousimis) was used to avoid the collapse of the pillars. In the case of DRIE, the microgels swollen in photoresist are used directly as the masks for etching. Contrary to MACE, DRIE is harsh with the mask and removes it overtime. In 30-45s the microgels are etched away. This constrains the maximum height of the pillars but also opens new possibilities on engineering the shape of the pillars as can be seen in Fig. S5, as once the microgel is etched away, the pillars start being etched into a tapered shape (see the pillars obtained with C3S0 microgels). On the other hand, DRIE produces a very homogeneous etching over the whole substrate, which it is a challenge for MACE.

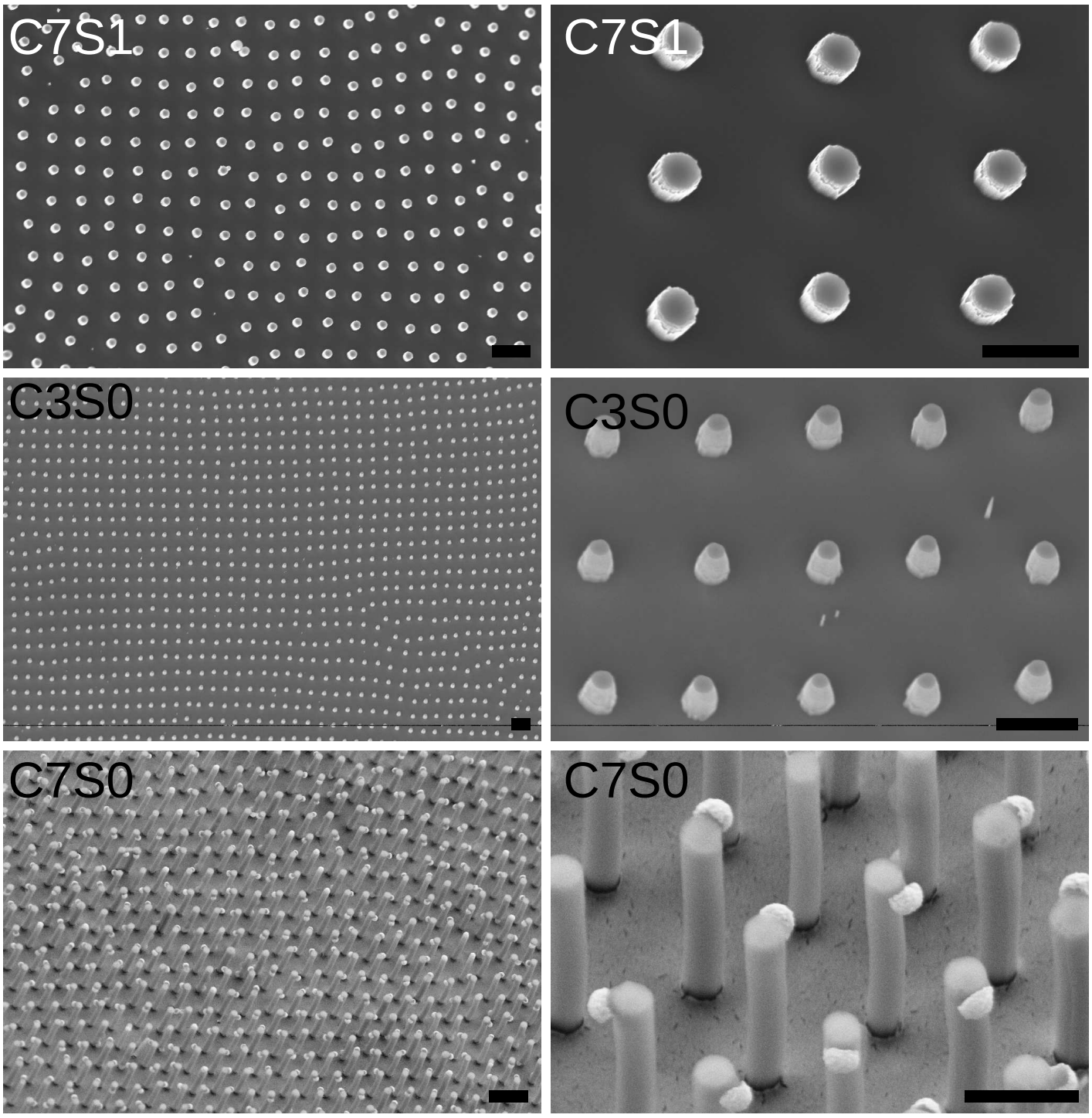

Figure S5: SEM images of vertically aligned nanowires obtained by soft colloidal lithography of square lattices deposited on silicon substrates. The substrates are tilted by 30° to quantify the height of the nanowires (right column). The substrate with C7S1 microgels was subjected to 45 s of dry etching (400nm pillars), the one with C3S0 to 30 s of dry etching (640nm pillars), and the one with C7S0 to 4 min of wet etching (2.6μm pillars). Scale bars are 2μm for the panels in the left and 1μm for the panels in the right.

Bibliography

[1] F. Camerin, M. A. Fernández-Rodríguez, L. Rovigatti, M.-N. Antonopoulou, N. Gnan, A. Ninarello, L. Isa and E. Zaccarelli, *ACS Nano*, 2019, **13**, 4548–4559.

[2] F. Grillo, M. A. Fernandez-Rodriguez, M.-N. Antonopoulou, D. Gerber and L. Isa, *Nature*, 2020, **582**, 219–224.

[3] M. Á. Fernández-Rodríguez, R. Elnathan, R. Ditcovski, F. Grillo, G. M. Conley, F. Timpu, A. Rauh, K. Geisel, T. Ellenbogen, R. Grange, F. Scheffold, M. Karg, W. Richtering, N. H. Voelcker and L. Isa, *Nanoscale*, 2018, **10**, 22189–22195.

[4] M. Rey, M. A. Fernandez-Rodriguez, M. Steinacher, L. Scheidegger, K. Geisel, W. Richtering, T. M. Squires and L. Isa, *Soft Matter*, 2016, **12**, 3545–3557.

[5] L. Scheidegger, M. Fernández-Rodríguez, K. Geisel, M. Zanini, R. Elnathan, W. Richtering and L. Isa, *Phys. Chem. Chem. Phys.*, 2017, **19**, 8671–8680.

[6] V. Ramasubramani, B. D. Dice, E. S. Harper, M. P. Spellings, J. A. Anderson and S. C. Glotzer, *Computer Physics Communications*, 2020, **254**, 107275.

[7] N. Vogel, J. Ally, K. Bley, M. Kappl, K. Landfester and C. K. Weiss, *Nanoscale*, 2014, **6**, 6879–6885.

[8] M. Rey, R. Elnathan, R. Ditcovski, K. Geisel, M. Zanini, M. A. Fernandez-Rodriguez, V. V. Naik, A. Frutiger, W. Richtering, T. Ellenbogen, N. H. Voelcker and L. Isa, *Nano Lett.*, 2016, **16**, 157–163.